Journal of Materials Science and Chemical Engineering, 2026, 14(11), 120-132
https://www.scirp.org/journal/msce
ISSN Online: 2327-6053
ISSN Print: 2327-6045

# Chemical, Granulochemical, and Mineralogical Characterization of Alumina Phosphates from Lam-Lam (Senegal)

**Mamadou Moustapha Diouf[1*], Emmanuelle Dosseh[1], Aminata Paye[1], Abdoul Aziz Ndiaye[2], Cheikhou Kane[1], Falilou Mbacké Sambe[1]**

[1]Laboratoire Eau, Énergie, Environnement et Procédés Industriels (LE3PI), École Supérieure Polytechnique (ESP), Université Cheikh Anta Diop de Dakar (UCAD), Dakar, Sénégal
[2]École Nationale Supérieure des Mines et de la Géologie (ENSMG), Université Cheikh Anta Diop de Dakar (UCAD), Dakar, Sénégal
Email: *mamadoumoustapha4.diouf@ucad.edu.sn

**How to cite this paper:** Diouf, M.M., Dosseh, E., Paye, A., Ndiaye, A.A., Kane, C. and Sambe, F.M. (2026) Chemical, Granulochemical, and Mineralogical Characterization of Alumina Phosphates from Lam-Lam (Senegal). *Journal of Materials Science and Chemical Engineering*, **14**, 120-132.
https://doi.org/10.4236/msce.2026.1411008

**Received:** October 23, 2026
**Accepted:** November 23, 2026
**Published:** November 26, 2026

Copyright © 2026 by author(s) and Scientific Research Publishing Inc.
This work is licensed under the Creative Commons Attribution International License (CC BY 4.0).
http://creativecommons.org/licenses/by/4.0/
Open Access

## Abstract

This study contributes to the characterization of Senegalese alumina phosphate ore. The objective is to identify its constituents and evaluate the feasibility of simultaneously preconcentrating phosphorus and aluminum. The methodological approach combines chemical and mineralogical analyses using X-ray fluorescence (XRF) and X-ray diffraction (XRD). It is supplemented by a microtextural study conducted using optical microscopy and a scanning electron microscope (SEM) coupled with energy-dispersive X-ray spectroscopy (EDS). Chemical analysis of the total rock reveals contents of 25.95% $P_2O_5$, 25.91% $Al_2O_3$, and 12.52% CaO, as well as a loss on ignition of 17.77%. The granulochemical analysis of seven size classes ranging from less than 0.63 mm to more than 10 mm shows an increase in the $P_2O_5$ content from 23.08% in the fine fraction (<0.63 mm) to 28.68% in the coarse fraction (>10 mm). The $Al_2O_3$ content remains close to that of $P_2O_5$ across all particle size classes. It ranges from 24.93% in the fine fraction to 28.75% in the coarse fraction. The 6.30 - 10 mm fraction contains 27.52% $P_2O_5$ and 26.17% $Al_2O_3$, along with the lowest $SiO_2$ content (2.52%). These observations suggest that the intermediate-to-coarse fractions are of interest for joint preconcentration tests of phosphorus and aluminum. XRD reveals a crystalline assemblage dominated by millisite (45.3%), crandallite (23.0%), and augelite (15.7%). Thin-section observations reveal a fine-grained matrix, heterogeneous porosity, and cracks. SEM observations reveal a heerogeneous microstructure, while spot EDS analyses distinguish, among other, alumino-calcium phosphate, siliceous, and aluminosilicate domains.

**Keywords**

Alumina Phosphates, Lam-Lam (Senegal), Granulochemistry, Chemical Characterization, Mineralogical Characterization

## 1. Introduction

Senegal's phosphate resources play a strategic role in the country's mining and agricultural economy [1] [2], and are characterized by great geological diversity [1] [3]. There are two main types of deposits: calcium phosphates [1] [3], and aluminum phosphates [1] [4]. The genesis of these deposits is part of the evolution of the Senegal-Mauritania-Guinea sedimentary basin [1] [5] [6], which is strongly influenced by continental and supergene weathering processes [7]-[10]. At Lam-Lam (Thiès region), these processes transform primary calcium phosphates into secondary aluminum compounds [4] [7] [11]. Flicoteaux *et al.* [4] and Vieillard *et al.* [7] have demonstrated that this weathering is accompanied by significant mobilization of calcium, silica, and aluminum. This phenomenon promotes the formation of complex mineral associations comprising fluorocarbonate apatites [3] [12], alumino-calcium phosphates (such as millisite and crandallite) [4] [7] [13], and aluminum phosphates [7] [11]. These transformations result not only in a profound change in the mineralogical composition [14], but also in a microtextural reorganization characterized by dissolution, the filling of porous spaces, and fracturing [7] [11]. However, despite their potential for chemical and industrial recovery [15] [16], the mineralogical complexity of alumina-phosphate ores poses a major challenge for their processing [13] [15] [17]. Thus, a thorough understanding of its mineralogy, microstructure, and the granulochemical distribution of its useful elements is necessary. This study is conducted within this context.

The study aims to further characterize the chemical, granulochemical, mineralogical, and microstructural properties of Senegalese alumina phosphate ore in order to:

- determine its chemical composition;
- identify fractions of potential interest for the joint preconcentration of phosphorus and aluminum;
- clarify the exact nature of its mineralogical composition as well as its microstructural organization.

To achieve this, the methodological approach combines chemical analysis of the whole rock, granulochemical analysis, X-ray diffraction, optical microscopy observations, and SEM-EDS analysis.

## 2. Materials and Methods

### 2.1. Raw Materials

The alumina phosphate deposits in Senegal are primarily located near the vil-

lages of Pallo and Lam-Lam, situated in the Mont Roland communes, Tivaoune Department, Thiès Region. Figure 1 shows an example of an outcrop of the deposit.



**Figure 1.** Example of an outcrop of the aluminium phosphate deposit.

Sampling was carried out at 16 outcrops in the Lam-Lam area. These outcrops were selected during the mapping of quarry outlines on the basis of their accessibility, spacing, and the presence of different stratigraphic levels. A total of 55 samples were collected from the different exposed facies of the series, excluding the cover soil, with 1 to 8 samples collected per outcrop. The samples were then mixed using 1 kg from each sample to prepare a composite sample. The composite sample subsequently underwent three preparation stages: homogenization, crushing, and sieving. Crushing was performed using a PEF 100 × 60 jaw crusher with a 15 mm discharge opening. Sieving was then carried out dry using a column of calibrated sieves, based on the principles of standard NF EN ISO 17892-4. This operation made it possible to separate seven grain-size classes: <0.63 mm; 0.63 - 1.25 mm; 1.25 - 1.60 mm; 1.60 - 3.15 mm; 3.15 - 6.30 mm; 6.30 - 10 mm; and >10 mm. The analyses were performed on the composite sample as well as on its different grain-size fractions. They therefore provide an overall characterization of the material but do not allow the variability between outcrops or between the sampled levels to be assessed.

### 2.2. Chemical Analyses of the Total Rock and Grain Size Fractions

The chemical composition was determined for the total rock (composite sample) as well as for the seven grain-size classes. All chemical analyses were performed by SGS South Africa. The oxides were determined by wavelength-dispersive X-ray fluorescence (WD-XRF) after lithium borate fusion, using the SGS reference method GOXRF72. Loss on ignition (LOI) was determined by gravimetry after calcination at 1000˚C, using the SGS reference method GPHY01V.

### 2.3. X-Ray Diffraction (XRD)

The identification of crystallized mineral phases was performed using Xray diffraction (XRD) with a Bruker D8 Advance diffractometer at the GET laboratory, University of Toulouse, France. Data were acquired in $\theta/2\theta$ mode, using CuK$\alpha$ radiation with a wavelength of $\lambda$ = 1.54060 Å. The phases were then identified by comparison with the ICDD (International Centre for Diffraction Data) database. Subsequently, a semi-quantitative (S-Q) estimation of the relative mass of the minerals was performed using the profile fit method. The reported mineral proportions refer to the identified crystalline phases and are normalized to 100% for this assemblage.

### 2.4. Optical Microscopy on Thin Sections

The petrographic and microtextural study was conducted using transmitted-light optical microscopy. The sample was first impregnated with a blue-stained epoxy resin to facilitate the visualization of porous spaces and fractures. The impregnated sample was then used to prepare a thin section. Images were acquired in unanalyzed polarized light (UPL) using a Nikon Eclipse E600POL polarizing microscope equipped with a digital camera. Observations focused on textures as well as the distribution of porosity and fractures.

### 2.5. Scanning Electron Microscopy and Microanalysis (SEM-EDS)

Elemental and textural microanalyses were performed using SEM-EDS on a polished thin section. The thin section was first coated with a conductive layer of carbon using an Eloise 208 Turbo Carbon Coater. The microscope used was a Tescan Vega 4 LMU operating in backscattered electron (BSE) mode, at an acceleration voltage of 15 kV and a working distance of 13.6 mm. The BSE images were used to examine the textures. Targeted EDS analyses were then performed to characterize each identified domain using a Bruker Quantax system equipped with a 30 mm² SDD detector. The spectra obtained allowed for a qualitative characterization of the elemental composition of the analyzed domains.

## 3. Results and Discussion

### 3.1. Experimental Results

The chemical composition of the total rock is presented in Table 1.

**Table 1.** Bulk-rock chemical composition.

| Components | Contents (%) |
|---|---|
| $P_2O_5$ | 25.95 |
| $Al_2O_3$ | 25.91 |
| CaO | 12.52 |
| $Fe_2O_3$ | 8.88 |
| $SiO_2$ | 3.81 |
| $TiO_2$ | 1.93 |
| $Na_2O$ | 1.04 |
| $Cr_2O_3$ | 0.16 |
| MgO | 0.11 |
| BaO | 0.10 |
| $K_2O$ | 0.06 |
| $V_2O_5$ | 0.06 |
| MnO | 0.02 |
| LOI | 17.77 |

The sample's $P_2O_5$ content, equal to 25.95%, confirms the phosphate nature of the ore. Furthermore, the $CaO/P_2O_5$ mass ratio, close to 0.48, suggests that phosphorus is likely not predominantly present in the form of calcium apatite. Indeed, for pure calcium fluorapatite, the $CaO/P_2O_5$ mass ratio is close to 1.3. The $Al_2O_3$ content, equal to 25.91%, confirms that this ore differs from slightly altered calcium phosphate ores and suggests that it belongs to a highly altered phosphate facies [4] [7]. Indeed, in slightly altered sedimentary phosphate ores, the main phosphate phase is generally apatite, often in the form of francolite [8]. In contrast, highly altered ores may be dominated by alumina-rich secondary phosphates such as crandallite and millisite [4] [7]. In summary, the chemical composition dominated by $P_2O_5$, $Al_2O_3$, and CaO, combined with the presence of $Fe_2O_3$ and $SiO_2$, indicates a complex alumino-calcium phosphate ore associated with a ferruginous and silicate matrix. The high loss on ignition (17.77%) suggests the presence of hydrated and hydroxylated minerals, such as, crandallite, millisite, kaolinite, and augelite. Indeed, these minerals contain hydroxyl groups and structural water, which result in mass losses due to dehydroxylation and dehydration during heating.

The $P_2O_5$ content of the Lam-Lam alumina phosphate (25.95%) is close to that of the Tobène calcium phosphate (26.00%), but higher than that of the alumina-rich sedimentary phosphate from Tapoa, Niger (18.20%) [1] [18]. In contrast, the $Al_2O_3$ contents and loss on ignition of Lam-Lam (25.91% and 17.77%, respectively) are similar to those of Tapoa (26.90% and 16.60% at 1000˚C) [18]. These observed contrasts may be related to the mineral phases and their evolution through weathering.

### 3.2. Chemical Composition by Particle Size

The chemical composition of the various grain size fractions studied (Table 2) shows that the $P_2O_5$ content increases with particle size. It ranges from 23.08% in the fine fraction (<0.63 mm) to 28.68% in the coarse fraction (>10 mm). This increase indicates a preferential concentration of phosphate constituents in the intermediate to coarse fractions. The $Al_2O_3$ contents remain essentially equal to those of $P_2O_5$ across all particle size classes. The maximum $Al_2O_3$ content (28.75%) is found in the coarse fraction, which also has the highest $P_2O_5$ content. This correlation supports the hypothesis of a joint concentration of phosphate and alumina phases in the coarse fractions. Unlike that of $P_2O_5$, the CaO content decreases with particle size. The $CaO/P_2O_5$ ratio therefore decreases as particle size increases. This trend is consistent with a relative increase in aluminum-rich, calcium-poor phosphate phases in the coarse fractions. Regarding silica, the $SiO_2$ content decreases gradually from 7.61% in the fine fraction (<0.63 mm) to 2.52% in the 6.30 - 10 mm fraction, then increases to 4.90% in the coarse fraction (>10 mm). This increase in the coarse fraction may indicate that certain phosphate aggregates remain associated with quartz particles or a silicate matrix. The $Fe_2O_3$ content varies between 7.74% and 10.49% depending on the fraction, indicating the presence of ferruginous phases in all fractions. These contents must be taken into account, as iron may constitute an impurity depending on the intended recovery process.

In all fractions, the minor oxides ($Cr_2O_3$, MgO, BaO, $K_2O$, $V_2O_5$ and MnO) have concentrations below 1%. $Na_2O$ and $TiO_2$, although slightly more abundant, remain minor constituents, with concentrations ranging from 0.87% to 1.21% and from 1.79% to 2.38%, respectively. Loss on ignition, meanwhile, ranges from 15.33% to 19.04%. This variation could be related to differing contributions from hydrated, hydroxylated, or from volatile matter, depending on the particle size fractions.

Table 2. Mass distribution and chemical composition of the different particle-size fractions.

| Components (%) | Grain size classes (mm) | | | | | | |
|---|---|---|---|---|---|---|---|
| | <0.63 | 0.63 - 1.25 | 1.25 - 1.60 | 1.60 - 3.15 | 3.15 - 6.30 | 6.30 - 10 | >10 |
| Mass fraction | 13.05 | 10.64 | 6.64 | 18.83 | 27.69 | 17.34 | 5.83 |
| $P_2O_5$ | 23.08 | 25.07 | 25.39 | 26.95 | 27.15 | 27.52 | 28.68 |
| $Al_2O_3$ | 24.93 | 25.58 | 25.51 | 26.34 | 25.84 | 26.17 | 28.75 |
| CaO | 13.34 | 12.63 | 12.10 | 11.75 | 11.70 | 11.00 | 7.78 |
| $Fe_2O_3$ | 7.74 | 9.09 | 9.15 | 9.63 | 9.84 | 10.49 | 9.51 |
| $SiO_2$ | 7.61 | 5.58 | 4.71 | 2.80 | 2.66 | 2.52 | 4.90 |
| $TiO_2$ | 1.79 | 1.84 | 1.86 | 1.91 | 1.98 | 2.08 | 2.38 |
| $Na_2O$ | 0.87 | 1.01 | 1.01 | 1.14 | 1.18 | 1.21 | 1.16 |
| $Cr_2O_3$ | 0.14 | 0.15 | 0.15 | 0.17 | 0.17 | 0.18 | 0.22 |

**Continued**

| | | | | | | | |
|---|---|---|---|---|---|---|---|
| MgO | 0.17 | 0.14 | 0.12 | 0.10 | 0.10 | 0.07 | 0.07 |
| BaO | 0.09 | 0.09 | 0.08 | 0.07 | 0.07 | 0.08 | 0.11 |
| $K_2O$ | 0.10 | 0.08 | 0.07 | 0.05 | 0.05 | 0.04 | 0.05 |
| $V_2O_5$ | 0.05 | 0.06 | 0.06 | 0.06 | 0.06 | 0.07 | 0.09 |
| MnO | 0.02 | 0.02 | 0.02 | 0.02 | 0.02 | 0.02 | 0.03 |
| LOI | 19.04 | 18.18 | 18.61 | 17.93 | 17.89 | 17.50 | 15.33 |

A comparison of the $P_2O_5$ and $Al_2O_3$ contents reveals that the difference between their concentrations remains less than 2% across all the fractions studied. Particle size classification therefore does not allow for the selective separation of phosphate and aluminum. Consequently, joint recovery of phosphate and alumina appears to be appropriate. To this end, the sum of $P_2O_5$ and $Al_2O_3$ can be used as a simple indicator of combined concentration. This sum is highest in the >10 mm fraction, at 57.43%, resulting from 28.68% $P_2O_5$ and 28.75% $Al_2O_3$. This fraction is therefore the richest from a strictly chemical standpoint. Nevertheless, the 6.30 - 10 mm fraction is the most favorable for joint preconcentration under practical conditions. It contains 27.52% $P_2O_5$ and 26.17% $Al_2O_3$, for a combined content of 53.69%. This fraction has the lowest silica content, at 2.52%. Its ratio ($P_2O_5$ + $Al_2O_3$)/$SiO_2$ reaches 21.31, the highest value among all fractions. Phosphate and alumina are therefore highly concentrated in this fraction, with minimal dilution by silica. The 3.15 - 6.30 mm size fraction is another interesting target. It combines high mass retention (27.69%) with good $P_2O_5$ (27.15%) and $Al_2O_3$ (25.84%) contents and low silica content (2.66%). It could be combined with the 6.30 - 10 mm fraction to form a composite 3.15 - 10 mm fraction, corresponding to a significant mass fraction of 45.03%, high phosphate and alumina contents, and a low silica content. It could be combined with the 6.30 - 10 mm fraction to form a 3.15 - 10 mm composite fraction, representing a significant mass yield of 45.03%. This preconcentrate exhibits high mass-weighted grades of 27.29% $P_2O_5$ (recovering 46.55% of the total $P_2O_5$) and 25.97% $Al_2O_3$ (recovering 44.98% of the total $Al_2O_3$), associated with a low silica content (2.61% $SiO_2$) and a mass-weighted iron content of 10.09% $Fe_2O_3$. This iron content should therefore be taken into account in subsequent beneficiation tests, as it may affect the quality of the preconcentrate depending on the intended use.

### 3.3. Mineralogical Characterization

The X-ray diffraction pattern (**Figure 2**) shows reveals a mineral assemblage composed primarily of millisite, crandallite, augelite, muscovite, quartz, kaolinite, and rutile.

The quantification results for the sample studied (**Table 3**) indicate that millisite is the dominant phase, followed by crandallite and augelite. The combined presence of these three phases confirms that phosphorus is primarily carried by calcium-aluminum and alumina phosphates.

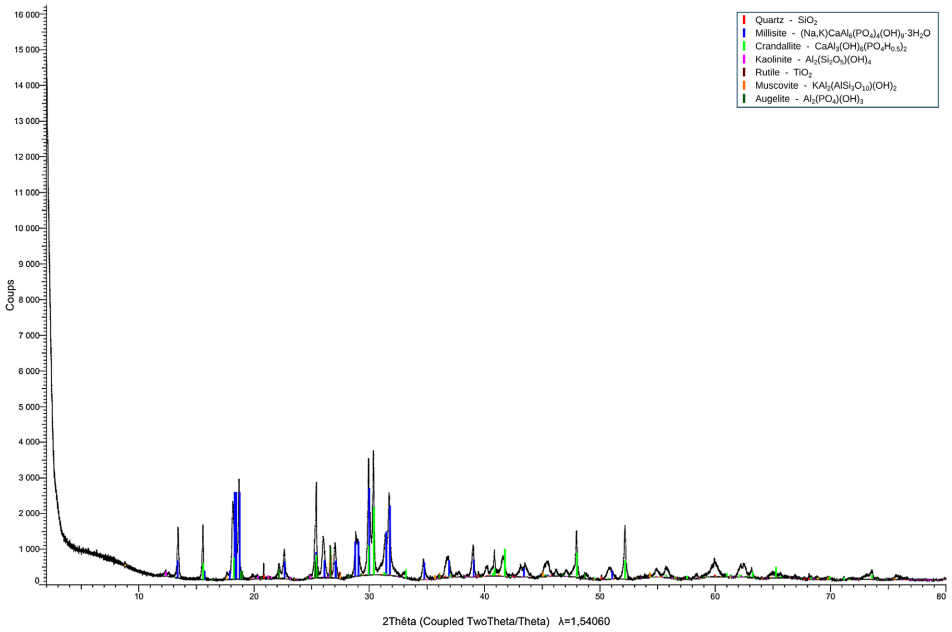



**Figure 2.** X-ray diffraction pattern.

**Table 3.** Identified and quantified mineralogical assemblage.

| Mineral phases | Contents (%) | Contents (%) |
|---|---|---|
| Millisite | $(Na,K)CaAl_6(PO_4)_4(OH)_9{\cdot}3H_2O$ | 45.3 |
| Crandallite | $CaAl_3(PO_4)_2(OH)_6$ | 23.0 |
| Augelite | $Al_2PO_4(OH)_3$ | 15.7 |
| Muscovite | $KAl_2(AlSi_3O_{10})\ (OH)_2$ | 9.1 |
| Quartz | $SiO_2$ | 3.5 |
| Kaolinite | $Al_2Si_2O_5(OH)_4$ | 2.6 |
| Rutile | $TiO_2$ | 0.9 |

Millisite, which accounts for 45.3% of the assemblage, is a hydrated aluminium-calcium phosphate; its predominance is consistent with the high contents of $P_2O_5$, $Al_2O_3$ and CaO determined by XRF. Its structure, containing hydroxyl groups and structural water, also contributes to the high loss on ignition observed. This phase is associated with crandallite (23.0%), which is a typical phase in the weathering profiles of sedimentary phosphates [7] [13], consistent with the descriptions of Lam-Lam by Flicoteaux *et al.* [11]. Augelite (15.7%) confirms that a significant proportion of the phosphate is present as aluminium phosphates. Muscovite (9.1%) is also identified as a minor phase. However, its estimated proportion is not fully consistent with the low $K_2O$ content (0.06%) measured by XRF. This phase may therefore be overestimated by the semi quantitative XRD procedure or misidentified. Finally, kaolinite (2.6%), quartz (3.5%) and rutile (0.9%) complete the mineralogical assemblage. These phases explain part of the silica, alumina and titanium contents measured by XRF.

Moreover, no distinct iron-bearing phase was identified by XRD, despite the $Fe_2O_3$ content of 8.88% determined by XRF. Iron is therefore likely hosted by ne-grained or poorly crystalline iron oxides or oxyhydroxides, such as hematite or goethite. These phases may not be detected or accurately quantified by XRD, particularly when they are nanometric, amorphous or poorly crystalline [19].

### 3.4. Thin-Section Characterization

The natural-light microphotographs shown in **Figure 3** reveal a fine, brownish-to-grayish phosphate matrix with domains of varying shapes and sizes. The blue resin highlights heterogeneous porosity, with openings of varying widths along the joints between the solid domains. These openings are accompanied by cracks traversing certain domains and by rounded to irregular cavities.

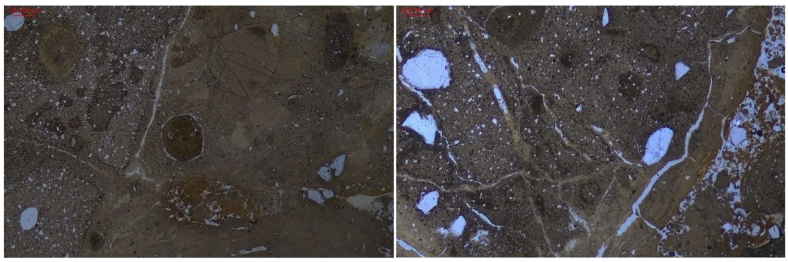


**Figure 3.** Natural-light microphotographs.

### 3.5. Morphological Characterization by SEM

The SEM image acquired in backscattered electron mode at 287 × reveals a highly heterogeneous microstructure of the alumina phosphate (**Figure 4**). The sample exhibits a fine matrix in which numerous grains and domains with varying morphologies and levels of contrast are dispersed. In particular, a marked textural contrast is observed between the two regions of the image: the upper part is characterised by a fine matrix rich in inclusions of varying sizes, whilst the lower region exhibits a coarser organisation with constituents of varied morphologies and dimensions. These contrasts primarily reflect local variations in composition.

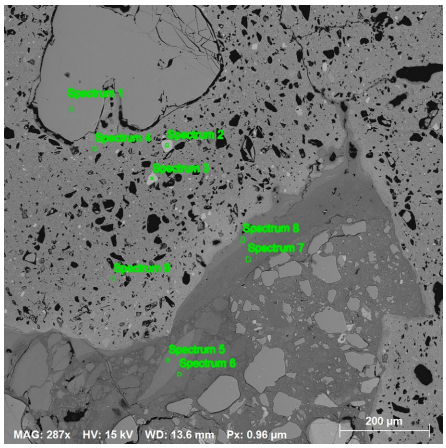



**Figure 4.** SEM image showing the locations of EDS spectra (Spectrum 1 to 9).

In order to determine the chemical nature of the different domains identified in the SEM image, nine-point elemental analyses using energy-dispersive X-ray spectrometry (EDS) were carried out (spectrum 1 to 9) (Figure 5).

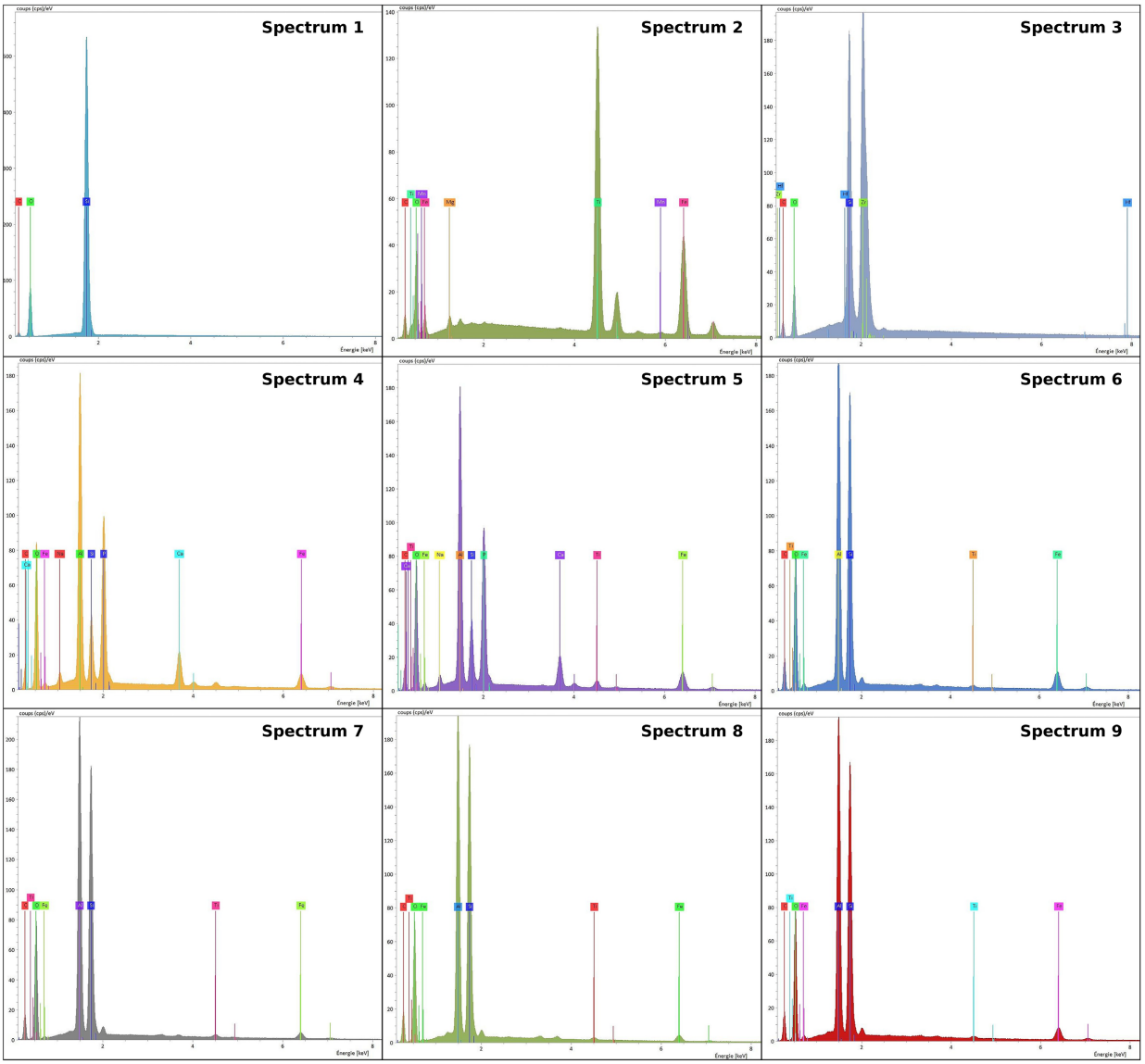



Figure 5. EDS spectra.

In spectrum 1, the silicon and oxygen signals are the strongest. They indicate a highly siliceous region, likely corresponding to a quartz grain, which is consistent with the presence of this phase identified by XRD.

Regarding spectrum 2, an intense titanium signal appears. It highlights a titanium-bearing region, consistent with the detection of rutile by XRD. The detection of iron, magnesium, and manganese in this region could be explained by a local association of the titanium-bearing constituent with other mineral phases.

Spectrum 3 reveals a zone containing zirconium, silicon, and hafnium. The detection of hafnium is consistent with the presence of zirconium. Indeed, these two

elements are frequently associated in zircon-bearing minerals [20].

Regarding spectrum 4 and 9, significant signals for aluminium, phosphorus and calcium are observed. These indicate the presence of aluminium-calcium phosphate domains. In addition to these elements, sodium and iron are present locally. The combination of phosphorus, aluminium and calcium is consistent with the presence of millisite and crandallite, as identified by XRD, whilst that of phosphorus and aluminium is consistent with the presence of augelite. These observations confirm the alumino-phosphate nature of the material.

Finally, in spectrum 5 to 8, the main signals are those of aluminium, silicon and oxygen. This combination indicates the presence of aluminosilicate domains.

## 4. Conclusion

The characterization of the alumina phosphate ore from Senegal reveals a chemical composition dominated by $P_2O_5$ (25.95%), $Al_2O_3$ (25.91%), CaO (12.52%), $Fe_2O_3$ (8.88%), and $SiO_2$ (3.81%), as well as a loss on ignition of 17.77%. The particle-size and chemical analysis shows an increase in the $P_2O_5$ content, which rises from 23.08% in the fine fraction (<0.63 mm) to 28.68% in the coarse fraction (>10 mm), while the CaO content decreases. $Al_2O_3$ remains abundant in all fractions and reaches a maximum content of 28.75% in the coarse fraction. This latter fraction thus has the highest contents of $P_2O_5$ and $Al_2O_3$. The 6.30 - 10 mm fraction, however, is distinguished by high $P_2O_5$ and $Al_2O_3$ contents, 27.52% and 26.17%, respectively associated with a minimum $SiO_2$ content of 2.52%. X-ray diffraction identifies a phase composition dominated by millisite (45.3%), crandallite (23.0%), and augelite (15.7%). Optical microscopy and SEM reveal a heterogeneous microstructure, comprising a fine matrix, domains of varying sizes and morphologies, porous spaces, and cracks. Spot EDS analyses highlight, among other features, aluminum-calcium phosphate, siliceous, and aluminosilicate domains.

## Author Contributions

**Conceptualization:** Mamadou Moustapha Diouf, Emmanuelle Dosseh, Ami nata Paye, cheikhou Kane, and Falilou Mbacké Sambe.

**Methodology:** Mamadou Moustapha Diouf, Emmanuelle Dosseh, Ami nata Paye, Cheikhou Kane, and Falilou Mbacké Sambe.

**Formal Analysis and Interpretation of Results:** Mamadou Moustapha Diouf.

**Investigation and Experimental Work**: Mamadou Moustapha Diouf and Emmanuelle Dosseh.

**Resources:** Abdoul Aziz Ndiaye and Cheikhou Kane.

**Data Curation:** Mamadou Moustapha Diouf and Aminata Paye.

**Writing Original Draft Preparation:** Mamadou Moustapha Diouf.

**Writing Review and Editing:** Mamadou Moustapha Diouf, Emmanuelle Dosseh, Aminata Paye.

**Visualization and Figure Preparation:** Mamadou Moustapha Diouf.

**Supervision**: Cheikhou Kane and Falilou Mbacké Sambe.

## Conflicts of Interest

The authors declare no conflicts of interest regarding the publication of this paper.

## References


[1] Prian, J. (2014) Phosphate Deposits of the Senegal-Mauritania-Guinea Basin (West Africa): A Review. *Procedia Engineering*, **83**, 27-36. https://doi.org/10.1016/j.proeng.2014.09.008

[2] Diallo, M. (2017) L'industrie du phosphate de Taïba au Sénégal: Front minier et tensions locales. *VertigO*, **28**. https://doi.org/10.4000/vertigo.18330

[3] Diagne, M., Fall, M., Diouf, M.B., Dione, N.P. and Samb, E.H.M. (2016) Mineralogical Characterisation of the Sedimentary Phosphate Deposit of Tobène (Western Senegal). *Journal of Shipping and Ocean Engineering*, **6**, 226-240. https://doi.org/10.17265/2159-5879/2016.04.005

[4] Flicoteaux, R., Nahon, D. and Paquet, H. (1977) Genèse des phosphates alumineux à partir des sédiments argilo-phosphatés du tertiaire de lam-lam (Sénégal). Suite minéralogique. Permanences et changements de structures. *Sciences Géologiques. Bulletin*, **30**, 153-174. https://doi.org/10.3406/sgeol.1977.1513

[5] Brancart, R. and Flicoteaux, R. (1971) Age des formations phosphatees de Lam Lam et de Taiba (Senegal occidental); Donnees micropaleontologiques, consequences stratigraphiques et paleogeographiques. *Bulletin de la Société Géologique de France*, **7**, 399-408. https://doi.org/10.2113/gssgfbull.s7-xiii.3-4.399

[6] Flicoteaux, R. (1975) Sur l'attribution a l'Eocene moyen des couches calcaires et argilo-phosphatees de Pallo (Plateau de Thies, Senegal occidental). *Bulletin de la Société Géologique de France*, **7**, 430-434. https://doi.org/10.2113/gssgfbull.s7-xvii.3.430

[7] Vieillard, P., Tardy, Y., and Nahon, D. (1979) Stability Fields of Clays and Aluminum Phosphates: Parageneses in Lateritic Weathering of Argillaceous Phosphate Sediments. *American Mineralogist*, **64**, 626-634. http://www.minsocam.org/ammin/AM64/AM64_626.pdf

[8] Lucas, J., Menor, E. and Prévôt, L. (1979) The Taïba Lime Phosphate Deposit (Senegal). An Example of Enrichment through Weathering. *Sciences Géologiques. Bulletin*, **32**, 39-57. https://doi.org/10.3406/sgeol.1979.1554

[9] Flicoteaux, R. and Lucas, J. (1984) Weathering of Phosphate Minerals. In: Nriagu, J.O. and Moore, P.B., Eds., *Photosphate Minerals*, Springer, 292-317. https://doi.org/10.1007/978-3-642-61736-2_9

[10] Altschuler, Z.S. (1973) The Weathering of Phosphate Deposits-Geochemical and Environmental Aspects. In: Griffith, E.J., Beeton, A., Spencer, J.M. and Mitchell, D.T., Eds., *Environmental Phosphorus Handbook*, Wiley, 33-96.

[11] Flicoteaux, R. (1982) Genesis of Aluminosilicate Phosphates in Western Senegal. Stages and Guidelines for Weathering. Geological Sciences. Institute of Geology-Louis Pasteur University, 270 p. https://www.persee.fr/doc/sgeol_0302-2684_1982_mon_67_1

[12] Nathan, Y. (1984) The Mineralogy and Geochemistry of Phosphorites. In: Nriagu, J.O. and Moore, P.B., Eds., *Photosphate Minerals*, Springer, 275-291. https://doi.org/10.1007/978-3-642-61736-2_8

[13] Toledo, M.C.M.D. (1999) Os fosfatos aluminosos da série da crandallita: uma revisão. *Revista do Instituto Geológico*, **20**, 49-63. https://doi.org/10.5935/0100-929x.19990005

[14] Dill, H.G. (2001) The Geology of Aluminium Phosphates and Sulphates of the Alunite Group Minerals: A Review. *Earth-Science Reviews*, **53**, 35-93. https://doi.org/10.1016/s0012-8252(00)00035-0

[15] Francisco, E.A.B., Prochnow, L.I., Toledo, M.C.M.D., Ferrari, V.C. and Jesus, S.L.D. (2007) Thermal Treatment of Aluminous Phosphates of the Crandallite Group and Its Effect on Phosphorus Solubility. *Scientia Agricola*, **64**, 269-274. https://doi.org/10.1590/s0103-90162007000300009

[16] Guardani, R., Drahos, J., Giulietti, M. and Schügerl, K. (1989) Studies on Calcination of Aluminium Phosphate Rock in Fluidized Bed Reactors. *Fertilizer Research*, **20**, 181-191. https://doi.org/10.1007/bf01054554

[17] Abouzeid, A.M. (2008) Physical and Thermal Treatment of Phosphate Ores—An Overview. *International Journal of Mineral Processing*, **85**, 59-84. https://doi.org/10.1016/j.minpro.2007.09.001

[18] Ousmane, M.S., Sanda, B.A., Mamane, S.A.A., Abdou, G.I., Zanguina, A. and Natatou, I. (2023) Physicochemical and Mineralogical Characterization of Natural Phosphate from Tapoa (Niger). *Journal of Materials and Environmental Science*, **14**, 1179-1186. https://www.jmaterenvironsci.com/Document/vol14/vol14_N11/JMES-2023-14115-Sani.pdf

[19] Choi, H., Han, M.S., Cho, N., Hwang, H., Sun, G.M. and Uhm, Y.R. (2025) Understanding the Corrosion Mechanism of Iron Artifacts Using Mössbauer Spectroscopy. *Scientific Reports*, **15**, Article No. 10207. https://doi.org/10.1038/s41598-025-95196-3

[20] Hoskin, P.W.O. (2003) The Composition of Zircon and Igneous and Metamorphic Petrogenesis. *Reviews in Mineralogy and Geochemistry*, **53**, 27-62. https://doi.org/10.2113/0530027